Journal of Magnetic Resonance 342 (2022) 107269

Contents lists available at ScienceDirect

Journal of Magnetic Resonance

journal homepage: www.elsevier.com/locate/jmr

An optimized quadrature RF receive coil for very-low-field (50.4 mT) magnetic resonance brain imaging

Sheng Shen [a], Xiaohan Kong [a], fanqin Meng [a], Jiamin Wu [b,c], Yucheng He [b], Pan Guo [d], Zheng Xu [a,*]

[a] State Key Laboratory of Power Transmission Equipment and System Security and New Technology, Chongqing University, Chongqing 400044, China
[b] Shenzhen Academy of Aerospace Technology, 6 Keji South 10th Road, Nanshan District, Shenzhen C4, 518057, China
[c] Harbin Institute of Technology, 92 Xi Da Zhi Jie, Harbin 150001, Nangang Qu, China
[d] School of Physics and Electronic Engineering, Chongqing Normal University, Chongqing 401331, China

ARTICLE INFO

Article history:
Received 10 February 2022
Revised 13 June 2022
Accepted 8 July 2022
Available online 14 July 2022

Keywords:
Very-low-field MRI
Quadrature RF coil
RF coil optimization

ABSTRACT

The radiofrequency (RF) receive coil is a direct probe for magnetic resonance imaging (MRI), and its performance determines the quality of MRI results. The RF coil employed for low-field MRI has a low working frequency, which makes its characteristic different from the RF coil exploited for conventional clinic MRI and may result in a different optimum RF coil configuration. To design and optimize a head RF receive coil for a very-low-field (50.4 mT) MRI system, we investigated the relationship between the structure and performance of the RF coil. Specifically, we focused on a quadrature RF coil consisting of a saddle coil and a modified Helmholtz coil wound around the surface of an elliptical cylinder. First, we evaluated the efficiency and RF magnetic field inhomogeneity of one-loop RF coil and determined the optimum dimension for saddle coil and modified Helmholtz RF coil. Then, we further studied the performance of the optimum-dimension RF coil from the perspective of the number of RF coil loops and revealed that the number of loops of RF coil for very-low-field MRI was a remarkable feature influencing the alternative current (AC) resistance of the RF coil and therefore make the SNR increase first and then decrease with the number of RF coil loops. We finally obtained the optimum number of loops for the saddle coil, modified Helmholtz coil, and fabricated a quadrature RF coil. The performance of the quadrature coil was evaluated through $CuSO_4$ phantom imaging and in vivo human brain imaging. In phantom imaging, the SNR of quadrature RF coil increased by about 40% compared with that of single-channel RF coil.

1. Introduction

The magnetic resonance imaging (MRI) technology has demonstrated its irreplaceable role in clinical diagnosis and scientific research. MRI at very low magnetic field (<100 mT) is an encouraging paradigm to enable low cost and mobile scanners [1–5]. However, opportunities at ULF have been neglected for many years because of low SNR. In recent years, with the development of low-noise hardware, computational MRI pulse sequences [6], and deep learning-based approaches to image formation [7,8], the performance of very-low-field MRI system has been significantly improved. In 2015, Sarracanie et al. reported a 6.5 mT MRI scanner used for rapid brain imaging [9]. In 2019, Mäkinen et al. used a hybrid MEG-ULF MRI system [10]. In 2020, Clarissa et al. presented their point-of-care MRI scanner, which is based on the Halbach Magnet [11].

In this work, we have focused on the RF receive coil for very-low-field brain MRI. The commonly used RF receive coil can be classified in accordance with the number of channels into three categories [12,13], namely, single-channel [14–17], quadrature [18,19], and phased array [20–22] RF coils. Single-channel RF coil includes solenoid RF coil, saddle RF coil, Helmholtz coil, and other RF coils with classical structure; has a simple structure; and can obtain relatively good imaging result with low hardware cost. Nevertheless, the single-channel RF coil may still be improved. The quadrature RF coil consists of two single-channel coils, and the RF magnetic field of each single-channel coil is perpendicular to each other. The SNR of a quadrature coil is effectively increased by adding another single-channel RF coil. The phased array RF coil is analogous to the array of radar and ultrasound and consists of several single-channel coils. Multichannel RF coil can significantly raise the SNR, and the phased array RF coil is the state-of-the-art technology of the RF receive coil for MRI. However, phased array RF coil has the drawbacks of complexity of structure and high hardware cost. Overall, the quadrature RF receive coil strikes a

* Corresponding author.
E-mail address: xuzheng@cqu.edu.cn (Z. Xu).

https://doi.org/10.1016/j.jmr.2022.107269
1090-7807/

good balance between hardware cost and performance and is still widely used in clinics and laboratory. We therefore intend to develop a quadrature RF receive coil for very-low-field brain MRI.

Objectively, the RF coil exploited in conventional clinical MRI has been well developed [23,24]. However, very-low-field MRI gives a low working frequency to the RF coil, and this discrepancy may result in different impedance characteristics of RF coil and implies that the optimum very-low-field RF coil may be different. Thus, we have investigated the alternative current (AC) resistance of very-low-field RF receive coil for brain imaging and optimized its structure in this work. Finally, the optimum structure of each single-channel RF coil of the quadrature coil is obtained and fabricated. We have also implemented phantom (cube phantom filled with $CuSO_4$ solution) imaging and calculated its SNR. We also implement in vivo brain imaging and obtained the T_1- and T_2-weighted brain images of a healthy volunteer.

In this work, we first studied the performance of a very-low-field RF coil from the perspective of the conductor density (number of RF coil loops) and reveal that the RF coil efficiency (defined by the average RF magnetic field generated by unit current) and resistance have different changing rates with the conductor density of RF coil (number of RF coil loops). This phenomenon implies that the wire winding pattern of RF coil can influence the AC resistance and significantly influence the SNR of RF coil. This result provides new evidence for low-field RF coil optimization.

2. Method and analysis

In this work, the quadrature RF coil to be optimized consists of a saddle coil and a modified Helmholtz coil. We first determine the dimension of the one-loop saddle RF coil and modified Helmholtz RF coil and then obtain the optimum number of RF coil loops by evaluating the SNR.

2.1. Dimension optimization

The quadrature RF receive coil is used for brain imaging. We wind the RF coil around the surface of an elliptical cylinder to fit the head and improve the filling factor. The Helmholtz coil is composed of two coaxial coils, where the radius of the coils is equal to the axial distance between the coils, we thus call the Helmholtz RF coil, wound around the elliptic cylinder, modified Helmholtz RF coil. The supporting former of RF coil with major axis of 125 mm, minor axis of 105 mm, and height of 240 is shown in Fig. 1(a). Fig. 1(b) shows the diagram of human brain imaging. Fig. 1(c) shows the diagram of ROI, which is a cylinder with a radius of 60 mm and height of 100 mm.

To obtain the optimum dimension parameters of saddle and modified Helmholtz RF coils, we calculate the coil efficiency and magnetic field inhomogeneity in the ROI, analyze their relationship, and finally obtain a set of optimum dimension parameters considering the constrain of the dimension of MRI scanner and the tradeoff between RF coil efficiency and RF field inhomogeneity.

The saddle RF coil wound around the surface of ellipse cylinder is described by angle (α) and length (L, Fig. 2[a]). Considering that the size of RF coil is much smaller than the length of electromagnetic wave at low frequency due to the very low main field (50.4 mT), we directly calculate the magnetic field of RF coil by using the Biot–Savart law. Hence, the RF magnetic field, $\boldsymbol{B1_s}$, in the ROI can be expressed as equation (1), $\boldsymbol{L_s}$ is the winding path of the saddle coil, r is the distance from the wire to target points in ROI, I is the exciting current of RF coil, and $\boldsymbol{e_r}$ is the unit vector pointing from RF coil to the target points in the ROI.

$$\boldsymbol{B1}_s(\alpha, L) = \int_{L_s(\alpha,\ L)} \frac{\mu_0 I}{4\pi} \frac{dl \times \boldsymbol{e_r}}{r^2} \tag{1}$$

The modified Helmholtz RF coil (Fig. 2[b]) is described by the gap (D) between two loops, and the RF magnetic field ($\boldsymbol{B1}_h$) is described as equation (2), where $\boldsymbol{L}_h$ is the winding path of the modified Helmholtz RF coil.

$$\boldsymbol{B1}_h(D) = \int_{L_h(D)} \frac{\mu_0 I}{4\pi} \frac{dl \times \boldsymbol{e_r}}{r^2} \tag{2}$$

The performance of a RF coil is parametrized by RF magnetic field inhomogeneity and SNR. In this work, the inhomogeneity of RF magnetic field is quantified by equation (3), which is the maximum relative error of RF magnetic field in the ROI. B_{max} and B_{min} are the RF magnetic field component's maximum and minimum values, respectively, that are perpendicular to the direction of the static main magnetic field. The SNR of RF coil is simply evaluated by equation (4), where $B1_{av}$ is the average value of magnetic field, and R is the AC resistance of RF coil. Ideally, we attempt to degrade the inhomogeneity of RF magnetic field and improve the SNR of RF coil simultaneously in RF coil optimization.

$$\delta = \left| \frac{B_{max} - B_{min}}{B_{max} + B_{min}} \right| \times 100\% \tag{3}$$

$$SNRs = \frac{B1_{av}}{I\sqrt{R}} \tag{4}$$

To optimize the structure of saddle RF coil preliminarily, we calculate the efficiency of RF coil and inhomogeneity of one-loop saddle RF coil with different structural parameters. Specifically, the range of α is set to 2°–180° with a step of 2°, and L is set to 2–240 mm with a step of 2 mm. A total of 10 800 structure combinations are calculated. We obtain the relationship between magnetic field inhomogeneity and one-loop RF coil efficiency (Fig. 3). The efficiency of RF coil is a rough estimation of the SNR. Basically, the RF magnetic field inhomogeneity decreases with RF coil efficiency, and we determine a working point with efficiency of 7.92 μT/A and inhomogeneity of 25.90%, which corresponds to structural parameters with α of 122° and L of 200 mm.

The modified Helmholtz RF coil is parameterized by D. We also calculate the efficiency and magnetic field inhomogeneity of the

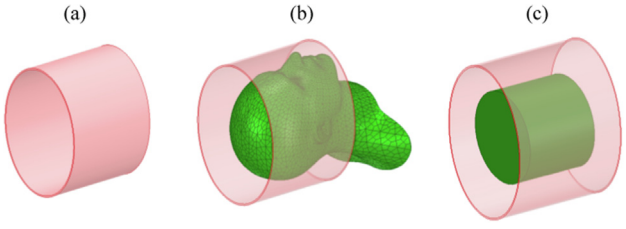

Fig. 1. Elliptical supporting former of the quadrature RF coil.

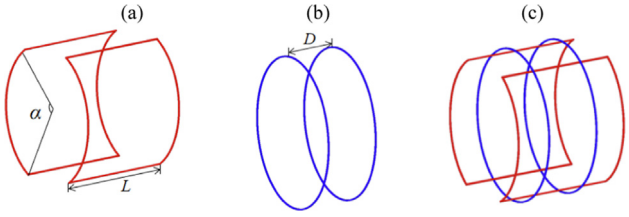

Fig. 2. (a) Saddle RF coil. (b) Modified Helmholtz RF coil. (c) Quadrature RF coil.

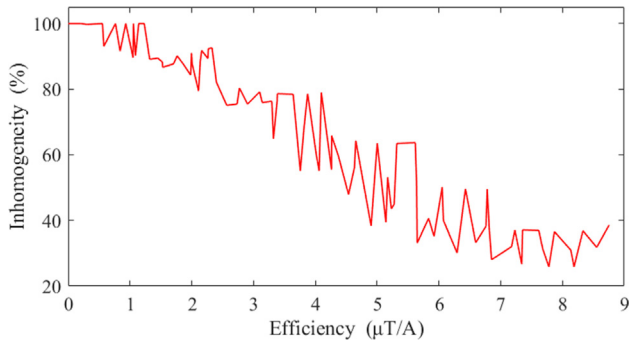

Fig. 3. Relationship between RF coil efficiency and RF field inhomogeneity (saddle RF coil).

modified Helmholtz RF coil. Specifically, we set the range of D as 1–240 mm with a step of 2 mm. The relationship between magnetic field inhomogeneity and one-loop modified Helmholtz RF coil efficiency is shown as Fig. 4, where the inhomogeneity of RF magnetic field increases first and then decreases with efficiency. We determine a working point with efficiency of 9.01 μT/A and inhomogeneity of 23.53%, which correspond to structural parameters with D of 66 mm. The working point with minimum RF magnetic field inhomogeneity is rejected in this work because of low efficiency, and we finally determine the working point with balance between efficiency and RF field inhomogeneity.

2.2. SNR optimization

In the *Dimension Optimization* part, we preliminarily obtain the optimum structure of one-loop RF coils. According to equation (4), the SNR of RF coil is dominated by magnetic field efficiency and AC resistance. For RF coil whose dimension has been determined, we can change its efficiency and AC resistance by adjusting the number of RF coil loops. At the same time, the magnetic field inhomogeneity is not significantly affected. Along with the changing number of RF coil loops, the changing rate of RF coil efficiency and AC resistance can be different, implying that the SNR of RF coil can be adjusted by changing its number of loops.

To investigate the relationship between the number of loops and the SNR of a RF coil for very-low-field MRI, we calculate the SNR of each single-channel RF coil of the quadrature RF coil. According to equation (4), we need to obtain RF coil efficiency and AC resistance in SNR calculation. The efficiency of the RF coil with different number of loops can be calculated precisely and efficiently by equations (1) and (2). Nevertheless, the AC resistance of a loaded RF coil is influenced by several factors and is challenging to obtain with an analytical expression or by a specific simulation model. In this work, the RF coil works in an MRI scanner, which consists of yoke, permanent magnet, anti-eddy plate, gradient coil system, and transmit coil (Fig. 5). These components of the MRI scanner and the patient to be scanned add to the AC resistance of RF coil by changing the surrounding magnetic permittivity, conductivity, and static background magnetic field of RF coil.

In this work, we measure the AC resistance of RF coil with different number of loops by using an impedance analyzer (Agilent, 429A, Califonia, the US), where $R_{unloaded}$ denotes the AC resistance measured on the bench (Fig. 6[a]), and R_{loaded} denotes the AC resistance measured with the RF coil in work condition (Fig. 6[b]).

Specifically, we adjust the number of loops of RF coil from 1 to 11, measure the unloaded and loaded AC resistance values of saddle and modified Helmholtz RF coils, and calculate the SNR by using equation (4). The measured parameters and normalized SNR are presented in Tables 1 and 2 and Fig. 6. $B1_{av}$ is the average value of magnetic field at target points in ROI, and R_{ratio} denotes the ratio of loaded and unloaded resistance values of the RF coil.

According to the magnetic field calculation result shown in Fig. 7(a), the efficiency of the RF coil basically increases linearly with the number of loops. According to the resistance measurement result shown in Fig. 7(b–c), the loaded and unloaded AC resistance values of RF coil increase with the number of loops, where the increase rate is also increasing. The loaded AC resistance is larger than unloaded AC resistance, basically below a factor of 3. The SNR of RF coils increases first and then decreases with the number of loops (Fig. 7[d]), implying that the optimum numbers of loops are around 5 and 3 for saddle and modified Helmholtz RF coils, respectively. We further analyze the parameters of RF coil with the number of loops of 2, 4, and 6, and SNR is presented as Fig. 8.

In accordance with the result shown in Fig. 8, we finally determine the optimum numbers of loops as 5 and 4 for saddle and modified Helmholtz RF coils, respectively.

By using the optimum dimension parameter and the optimum number of loops, we fabricate an optimum quadrature RF receive coil (Fig. 9[a]) and tune and match two single-channel RF coils of quadrature coil utilizing π-shaped circuit (Fig. 9[b]).

After tuning and matching, we measure (Vector net analyzer, ZND, R&S, Munich, Germany) the S11 and S22 parameters of modified Helmholtz and saddle RF coils and S12 parameters between them. The measurement result is shown as Fig. 10. S11, S22, and S12 are −23.08, −25.21, and −16.32 dB, respectively.

2.3. Consent and ethics committee

This experimental study was approved by the Ethics Committee of Southwest Hospital. Informed consent was obtained from imaging subjects and healthy volunteers. MRI imaging was performed using approved guidelines and regulations.

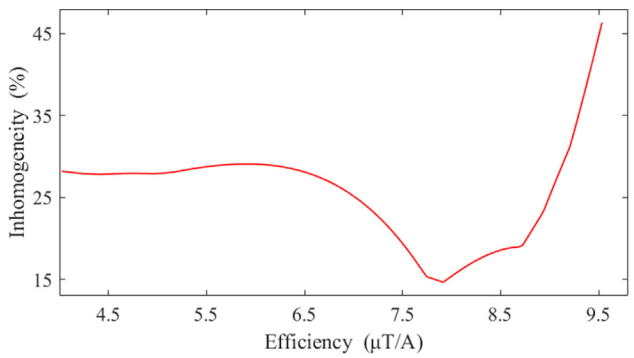

Fig. 4. Relationship between RF coil efficiency and RF field inhomogeneity (Modified Helmholtz RF coil).

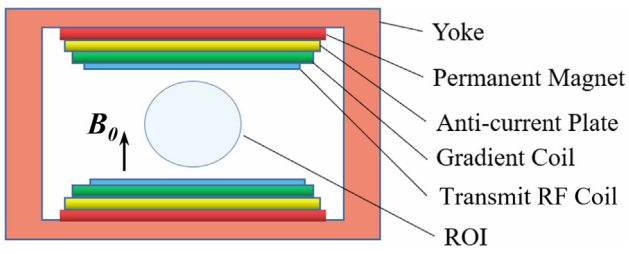

Fig. 5. Diagram of the permanent-magnet MRI scanner. B_0 denotes the static main field of the scanner.

Fig. 6. AC resistance measurement. (a) Unloaded RF coil. (b) Loaded RF coil.

Table 1
Parameters of saddle RF coil.

	1	3	5	7	9	11
$B1_{av}$ ($\mu T/A$)	7.40	21.84	35.79	49.26	62.21	74.62
$R_{unloaded}$ (Ω)	0.83	1.62	3.31	7.82	15.91	42.67
R_{loaded} (Ω)	0.88	2.27	4.95	12.78	40.27	65.96
R_{ration}	1.06	1.40	1.50	1.63	2.53	1.55
Normalized SNR	0.49	0.90	1	0.85	0.61	0.57

Table 2
Parameters of modified Helmholtz RF coil.

	1	3	5	7	9	11
$B1_{av}$($\mu T/A$)	9.15	27.81	46.93	66.45	86.35	106.57
R_{unload} (Ω)	0.69	2.44	4.04	9.18	30.02	66.45
R_{load} (Ω)	0.80	2.97	10.03	20.33	64.16	172.01
R_{ratio}	1.16	1.22	2.48	2.21	2.14	2.59
Normalized SNR	0.63	1.00	0.92	0.91	0.67	0.55

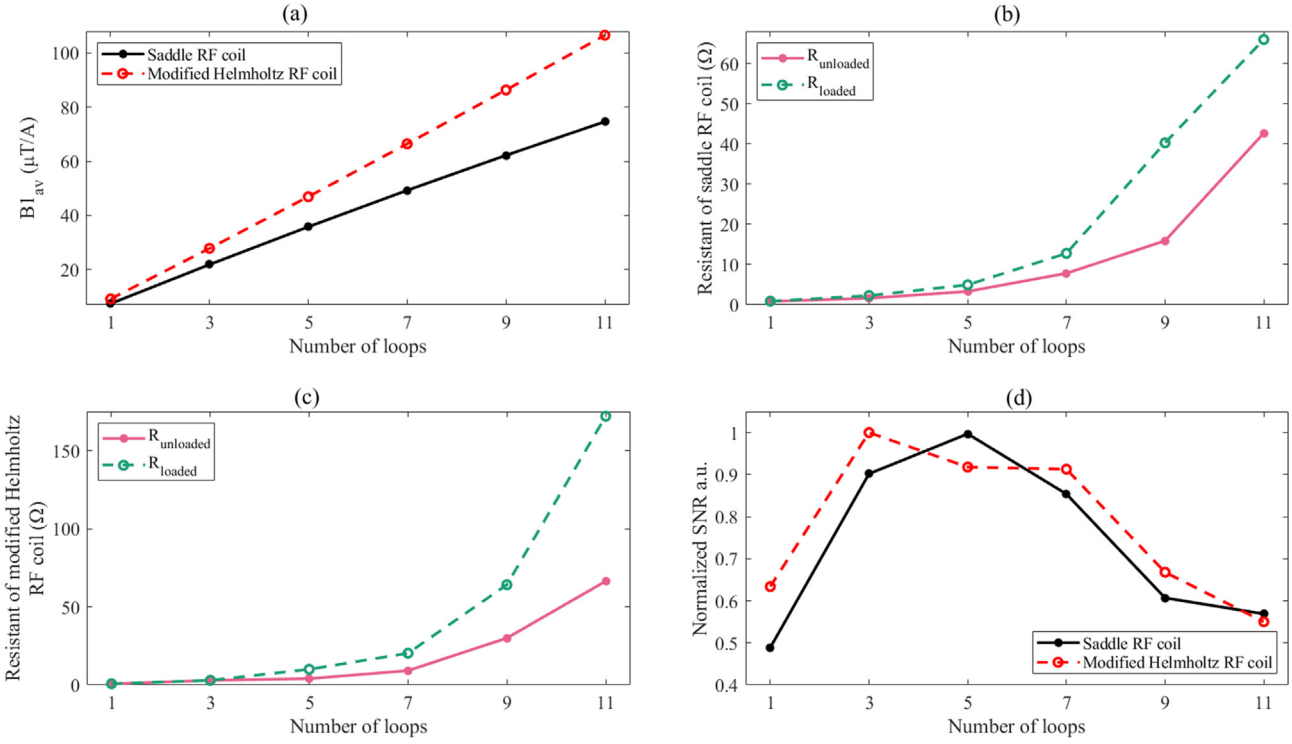

Fig. 7. Parameters of saddle and modified Helmholtz RF coils.

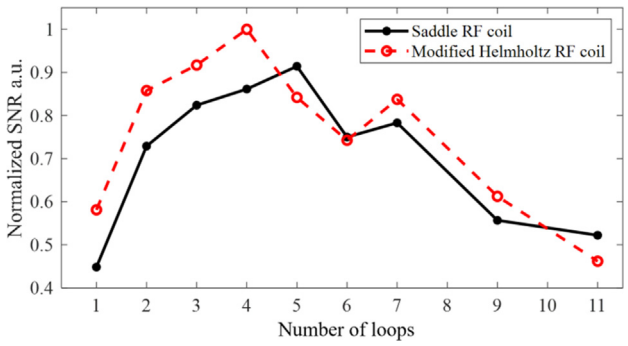

Fig. 8. SNR of saddle and modified Helmholtz RF coils.

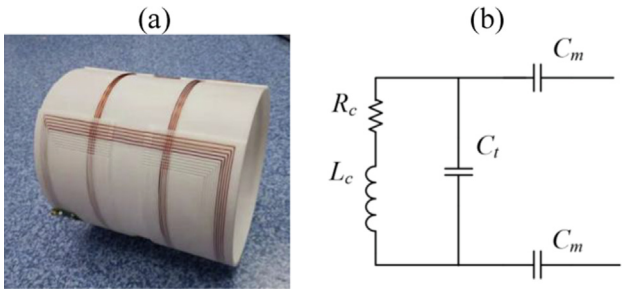

Fig. 9. (a) Optimum quadrature RF coil prototype. (b) π-shaped RF circuit for tuning and matching.

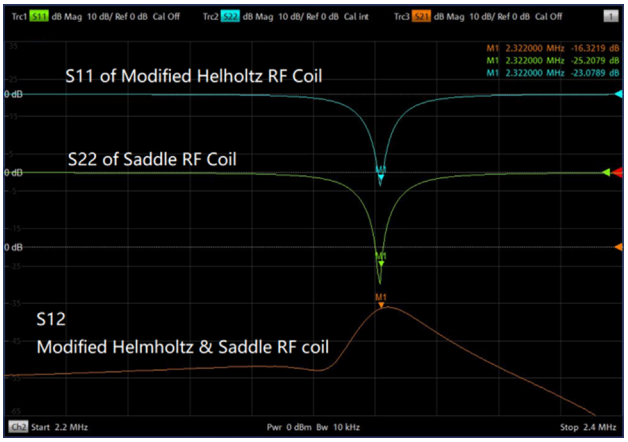

Fig. 10. S11 and S12 measurement of the quadrature RF coil.

3. Experiments and results

3.1. Phantom imaging

With the optimum quadrature RF coil, we implement phantom imaging. The cube phantom with geometric structure inside is filled with $CuSO_4$ solution (1.95 mg/mL, Fig. 11[a–b]). The transmit RF coil of the scanner is shown as Fig. 11(c). We scan the phantom using gradient echo (GRE) sequence with voxel matrix of 128 × 128 × 10, voxel dimension of 1.5 mm × 1.5 mm × 10 mm, flip angle of 90°, and an average number of 2. Imaging results are obtained in 2 min and 45 s (Fig. 12).

In Fig. 12, the composed image is obtained by solving the root of the square sum of pixel value of images obtained by saddle and modified Helmholtz RF coils. We calculate the SNR of each image shown in Fig. 12, and the normalized SNR of each image is shown in Table 3 and Fig. 13. The SNR of image is defined as the ratio of average pixel value in the center and standard deviation of pixel value at the edge of the image. The SNR of the composed image is significantly increased by approximately by 40%, and the SNR of the optimized modified Helmholtz RF coil is slightly better than that of saddle RF coil.

3.2. In vivo human brain imaging

We scan the brain of a healthy volunteer by using GRE sequence with resolution matrix of 128 × 128 × 10, resolution dimension of 2 mm × 2 mm × 10 mm, flip angle of 30°, and average number of 4. Imaging results (T_1-weighted brain images) are obtained in 5 min and 29 s (Fig. 14).

We also scan the brain of a healthy volunteer by using a fast spin-echo (FSE) sequence with resolution matrix of 176 × 120 × 8, voxel dimension of 1.5 mm × 2 mm × 8 mm, and average number of 4. Imaging results (T_1-weighted brain images) are obtained in 7 min (Fig. 15).

4. Discussion

In this work, we intend to develop an optimum quadrature RF receive coil for brain imaging at very low field. In the beginning, we apply the conclusion in [25], which implies that a large number of RF coil loops results in high SNR. However, our preliminary experiment, which compares the imaging results obtained with 10- and 20-turn solenoid RF coil, does not support this conclusion, where the SNR of images obtained by 10-turn solenoid RF coil is high. Then, we realize that our scanner structure and the background magnetic field of the scanner is different from that in [25], which may result in different characteristics of the RF coil in our work.

The preliminary imaging experiment suggests that the number of loops of RF coil can be a factor influencing the SNR of MRI. We therefore evaluate the SNR of an RF coil with different numbers of loops. In SNR evaluation, the AC resistance measurement is challenging. Given that the impedance angle of RF coil is close to 90°, the minute error in impedance angle results in a significant change in the horizontal component of the impedance, i.e., AC resistance. In the measurement, we even obtain minus AC resistance value with an impedance analyzer. Finally, we connect the capacitor in series with RF coil, resonate the RF coil at the Lamour frequency of MRI scanner, and measure the AC resistance of RF coil properly.

According to the parameters shown in Tables 1 and 2. The R_{ratio} of RF coil for very-low-field (50.4 mT) MRI is basically below 3 and is significantly smaller compared with that of the RF coil for conventional high-field MRI, which is usually higher than 5 or more [12,26,27]. This evidence underlines the impedance difference of RF coil between high- and very-low-field MRI. Additionally, a new unknown point for RF coil design emerges from our present work. The conductor pattern of RF coil can influence the RF magnetic field distribution and RF coil impedance simultaneously, where the impedance is determined by the material of conductor, the structure of RF coil, and the RF magnetic field distribution. The influence of the conductor pattern of an RF coil on its impedance and RF magnetic field will be quantified and included in the RF coil optimization in future studies.

5. Summary and conclusion

We optimize and fabricate a quadrature receive RF coil for brain imaging, which consists of a saddle and modified Helmholtz RF coils. Finally, phantom imaging and in vivo human brain imaging are implemented using this quadrature RF coil. In this work,

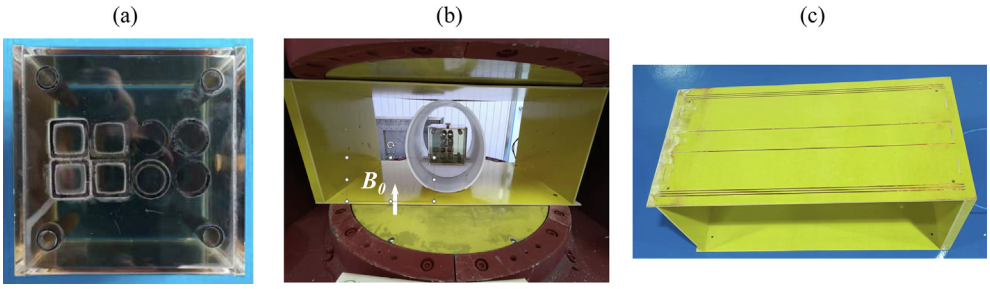

Fig. 11. Phantom Imaging. (a) Diagram of the cube phantom. (b) Cube phantom to be scanned in the MRI scanner. (c) Transmit RF coil of the MRI scanner.

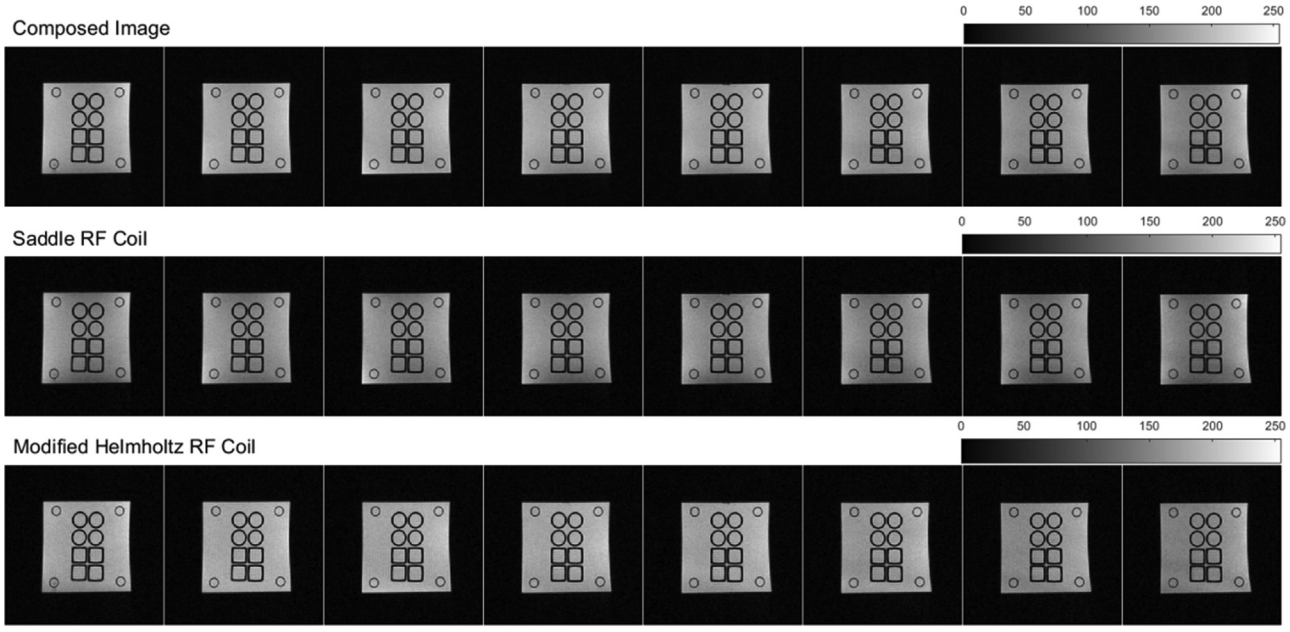

Fig. 12. Imaging results of the phantom.

Table 3
Normalized SNR of images in Fig. 12.

	1	2	3	4	5	6	7	8
Modified Helmholtz RF Coil	0.69	0.75	0.72	0.70	0.71	0.66	0.66	0.60
Saddle RF Coil	0.69	0.72	0.67	0.62	0.63	0.61	0.62	0.55
Composed	0.96	1.00	0.94	0.95	0.92	0.84	0.88	0.80

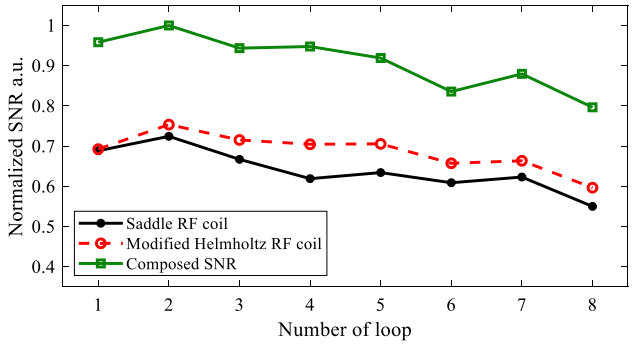

Fig. 13. Normalized SNR of images shown in Fig. 12.

we first analyze, optimize RF coil from the perspective of the number of RF coil loops, and reveal that the number of loops is a significant factor influencing the SNR of RF coil for very-low-field MRI (50.4 mT), providing new evidence for RF coil design and optimization.

Declaration of Competing Interest

The authors declare that they have no known competing financial interests or personal relationships that could have appeared to influence the work reported in this paper.

Acknowledgment

This work is supported by the National Natural Science Foundation of China (52077023), Natural Science Foundation of Chongqing (cstc2020jcyj-msxmX0340), and Shenzhen Science and Technology Innovation Commission (CJGJZD20200617102402006). The authors would like to thank Wei Zhang for the help he provided in RF coil impedance measurement.

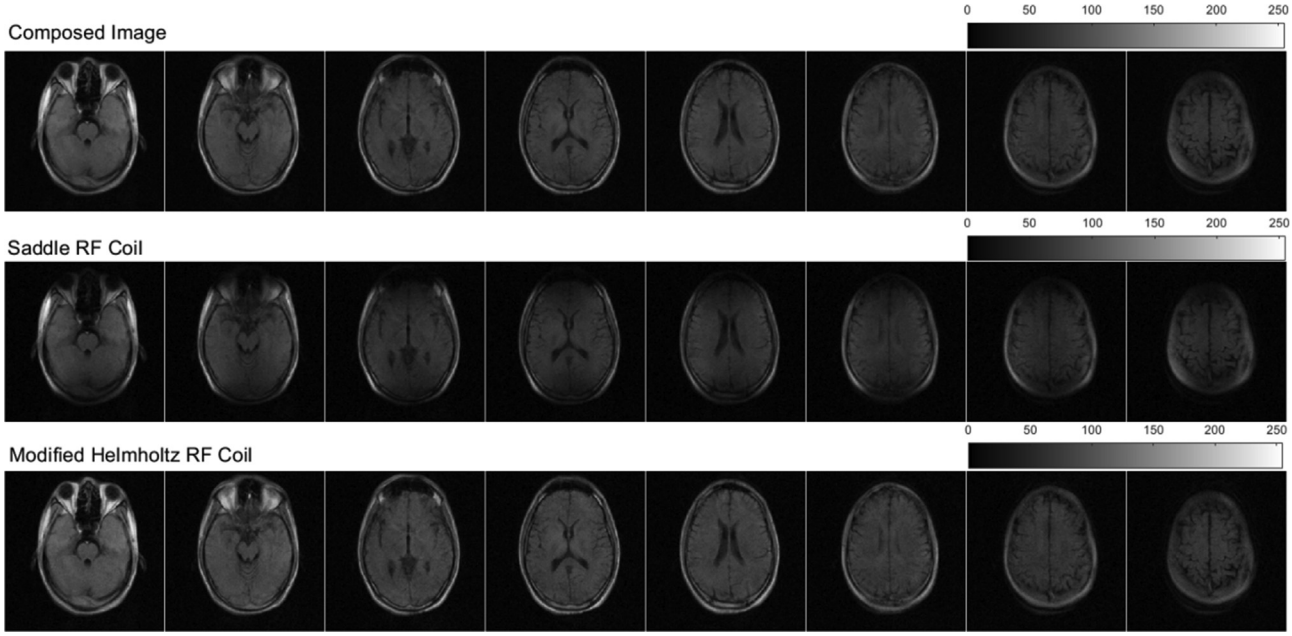

Fig. 14. Human brain images obtained using the GRE sequence.

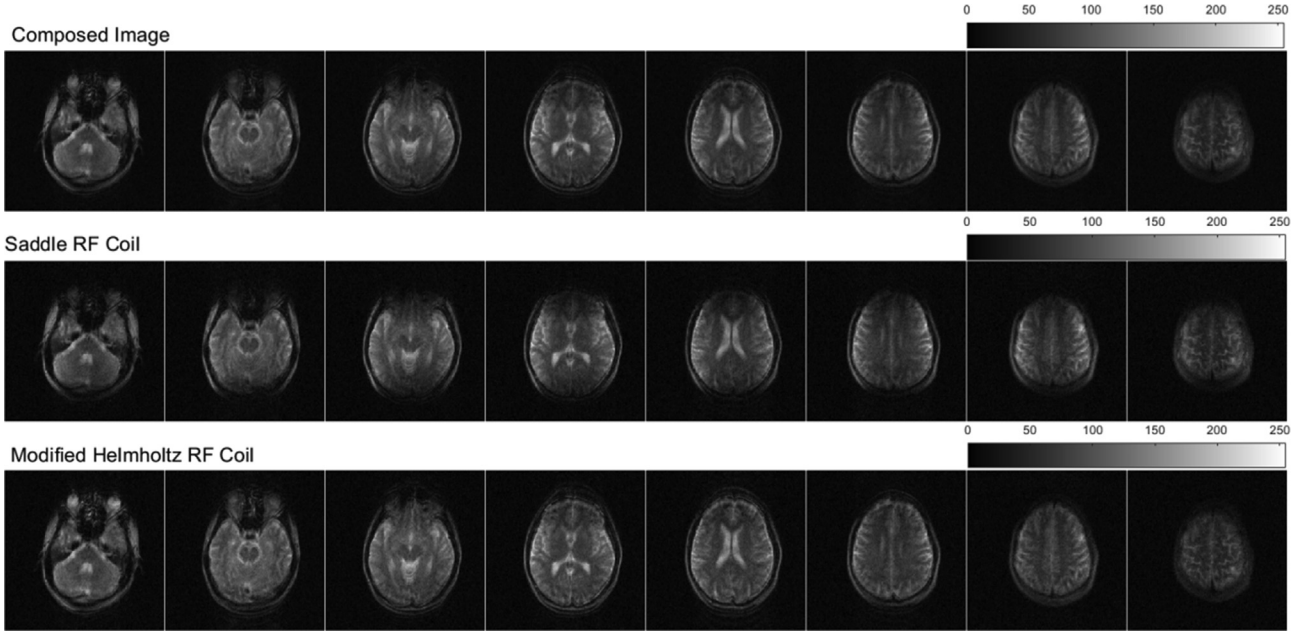

Fig. 15. Human brain images obtained using the FSE sequence.

References

[1] L.L. Wald, P.C. McDaniel, T. Witzel, J.P. Stockmann, C.Z. Cooley, Low-cost and portable MRI, J. Magn. Reson. Imaging 4 (3) (Oct. 2019) 31.
[2] Y. He, W. He, L. Tan, et al., Use of 2.1 MHz MRI scanner for brain imaging and its preliminary results in stroke, J. Magn. Reson. 319 (2020) 106829, https://doi.org/10.1016/j.jmr.2020.106829.
[3] J.P. Marques, F.F.J. Simonis, A.G. Webb, Low- field MRI: An MR physics perspective, J. Magn. Reson. Imaging 58 (Jan. 2019) 1182.
[4] K.N. Sheth et al., Assessment of Brain Injury Using Portable, Low-Field Magnetic Resonance Imaging at the Bedside of Critically Ill Patients, Jama Neurol. 78 (1) (Sep. 2020) 41–47, https://doi.org/10.1001/jamaneurol.2020.3263.
[5] M.H. Mazurek et al., Portable, bedside, low-field magnetic resonance imaging for evaluation of intracerebral hemorrhage, Nat. Commun. 12 (1) (2021) 5119, https://doi.org/10.1038/s41467-021-25441-6.
[6] D. Ma, V. Gulani, N. Seiberlich, K. Liu, J.L. Sunshine, J.L. Duerk, M.A. Griswold, Magnetic resonance fingerprinting, Nature 495 (2013) 187–192.
[7] B. Zhu, J.Z. Liu, S.F. Cauley, B.R. Rosen, M.S. Rosen, Image reconstruction by domain-transform manifold learning, Nature 555 (7697) (Mar. 2018) 487–492.
[8] N. Koonjoo, B. Zhu, G.C. Bagnall, D. Bhutto, M.S. Rosen, Boosting the signal-to-noise of low-field MRI with deep learning image reconstruction, Sci. Rep. 11 (1) (Apr. 2021) 8248, https://doi.org/10.1038/s41598-021-87482-7.
[9] M. Sarracanie, C.D. LaPierre, N. Salameh, D.E.J. Waddington, T. Witzel, M.S. Rosen, Low-Cost High-Performance MRI, Sci. Rep. 5 (1) (Oct. 2015) 15177.
[10] A.J. Mäkinen, K.C.J. Zevenhoven, R.J. Ilmoniemi, Automatic Spatial Calibration of Ultra-Low-Field MRI for High-Accuracy Hybrid MEG–MRI, IEEE Trans. Med. Imaging 38 (6) (June 2019) 1317–1327.
[11] C.Z. Cooley, P.C. McDaniel, J.P. Stockmann, et al., A portable scanner for magnetic resonance imaging of the brain, Nat. Biomed. Eng. 5 (2021) 229–239.
[12] B. Gruber, M. Froeling, T. Leiner, D.W.J. Klomp, RF coils: A practical guide for non-physicists, J. Magn. Reson. Imaging 48 (3) (2018 Jun 13) 590–604.
[13] J.R. Griffiths, RF Coils for MRI, Proteomics (2012).

[14] H.S. Lee, D.C. Woo, K.H. Min, et al., Development of a solenoid RF coil for animal imaging in 3 T high-magnetic-field MRI, Scanning 30 (5) (2008) 419–425.
[15] B. Blasiak, V. Volotovskyy, R. Tyson, et al., An RF breast coil for 0.2 T MRI, Concepts Magn. Reson. Part B: Magnetic Reson. Eng. 46 (1) (2016) 3–7.
[16] G. Giovannetti, F. Frijia, A. Flori, et al., Design and simulation of a Helmholtz coil for Magnetic Resonance Imaging and Spectroscopy experiments with a 3T MR clinical scanner, Appl. Magn. Reson. 50 (9) (2019) 1083–1097.
[17] G. Giovannetti, F. Frijia, S. Attanasio, et al., Magnetic resonance butterfly coils: Design and application for hyperpolarized 13C studies, Measurement 46 (9) (2013) 3282–3290.
[18] V.J. Sank, C.N. Chen, D.I. Hoult, A quadrature coil for the adult human head, J. Magn. Reson. 69 (2) (1986) 236–242.
[19] A. Rustemi, V. Boer, V. Zhurbenko, Design of a quadrature coil for MRI of carbon in human liver at 7T, 2020 14th European Conference on Antennas and Propagation (EuCAP). IEEE, 2020, 1-4.
[20] P.B. Roemer, W.A. Edelstein, C.E. Hayes, et al., The NMR phased array, Magn. Reson. Med. 16 (2) (1990) 192–225.
[21] M. Schmitt, A. Potthast, D.E. Sosnovik, et al., A 128-channel receive-only cardiac coil for highly accelerated cardiac MRI at 3 Tesla, Magn. Reson. Med.: An Official J. Int. Soc. Magn. Reson. Med. 59 (6) (2008) 1431–1439.
[22] C.J. Hardy, R.O. Giaquinto, J.E. Piel, et al., 128-channel body MRI with a flexible high-density receiver-coil array, J. Magn. Reson. Imaging: An Official J. Int. Soc. Magn. Reson. Med. 28 (5) (2008) 1219–1225.
[23] B.G. Lawrence, S. Crozier, D.D. Yau, et al., A time-harmonic inverse methodology for the design of RF coils in MRI, IEEE Trans. Biomed. Eng. 49 (1) (2002) 64–71.
[24] Fujita, L.S. Petropoulos, M.A. Morich, S.M. Shvartsmen, R.W. Brown, A hybrid inverse approach applied to the design of lumped-element RF coils, in IEEE Transactions on Biomedical Engineering, vol. 46, no. 3, pp. 353-361, March 1999, doi: 10.1109/10.748988.
[25] S. Shen, Z. Xu, N. Koonjoo, et al., Optimization of a Close-Fitting Volume RF Coil for Brain Imaging at 6.5 mT Using Linear Programming, IEEE Trans. Biomed. Eng. 68 (4) (2020) 1106–1114.
[26] H. Wen, A.S. Chesnick, R.S. Balaban, The design and test of a new volume coil for high field imaging, Magn. Reson. Med. 32 (4) (1994) 492–498.
[27] P. Vernickel, P. Röschmann, C. Findeklee, K.M. Lüdeke, C. Leussler, J. Overweg, U. Katscher, I. Grässlin, K. Schünemann, Eight-channel transmit/receive body MRI coil at 3T, Magn. Reson. Med.: An Official J. Int. Soc. Magn. Reson. Med. 58 (2) (2007) 381–389.